DMD Fast Forward. Published on September 8, 2008 as doi:10.1124/dmd.108.023770




# Key Residues Controlling Phenacetin Metabolism by Human Cytochrome P450 2A Enzymes[†]

**Natasha M. DeVore, Brian D. Smith, Michael J. Urban, and Emily E. Scott***

Department of Medicinal Chemistry, University of Kansas, 1251 Wescoe Hall Dr., Lawrence, KS 66045

**Running title:** Key residues for phenacetin metabolism in human cytochrome P450 2A enzymes

**Corresponding author:** Emily E. Scott, Ph.D., Department of Medicinal Chemistry, University of Kansas, 1251 Wescoe Hall Dr., Lawrence, KS 66045, Tel. 785 864-5559; Fax. 785 864 5326; E-mail: eescott@ku.edu

**Counts:**

# of text pages: 20

# of tables: 6

# of figures: 7

# of references: 29

# of words in:

Abstract: 230

Introduction: 539

Discussion: 1,349

Nonstandard abbreviations: Cytochrome P450 (CYP)

**Abstract**

Cytochrome P450s (CYP) metabolize a large number of diverse substrates with specific regio- and stereo-specificity. A number of compounds, including nicotine, cotinine, and aflatoxin $B_1$, are metabolites of the 94% identical CYP2A13 and CYP2A6 enzymes but at different rates. Phenacetin and 4-aminobiphenyl were identified as substrates of human cytochromes P450 1A2 and 2A13, but not of CYP2A6. The purpose of this study is to identify active site amino acids that are responsible for CYP2A substrate specificity using phenacetin as a structural probe. Ten amino acid residues that differ in the CYP2A13 and CYP2A6 active sites were exchanged between the two enzymes. Phenacetin binding revealed that the six substitutions CYP2A13 S208I, A213S, F300I, A301G, M365V, and G369S decreased phenacetin affinity. While incorporation of individual CYP2A13 residues into CYP2A6 had little effect on this enzyme's very low levels of phenacetin metabolism, the combination of double, triple, and quadruple substitutions at positions 208, 300, 301, and 369 increasingly endowed CYP2A6 with the ability to metabolize phenacetin. Enzyme kinetics revealed that the CYP2A6 I208S/I300F/G301A/S369G mutant protein *O*-deethylated phenacetin with a $K_m$ of 10.3 μM and a $k_{cat}$ of 2.9 $min^{-1}$, which compare very favorably with CYP2A13 ($K_m$ 10.7 μM, $k_{cat}$ 3.8 $min^{-1}$). A 2.15 Å crystal structure of the mutant CYP2A6 I208S/I300F/G301A/S369G protein with phenacetin in the active site provided a structural rationale for the differences in phenacetin metabolism between CYP2A6 and CYP2A13.

DMD Fast Forward. Published on September 8, 2008 as DOI: 10.1124/dmd.108.023770
This article has not been copyedited and formatted. The final version may differ from this version.



**Introduction**

The functional human cytochrome P450 2A enzymes include CYP2A13, which is primarily expressed within the respiratory tract with the highest level of mRNA in nasal mucosa, and CYP2A6, which contributes to 1 – 10% of the total P450 in the liver (Su et al., 2000; Zhang et al., 2006). These enzymes metabolize a variety of small cyclic compounds including coumarin, nicotine, aflatoxin $B_1$ ($AFB_1$), naphthalene, styrene, toluene, 4-aminobiphenyl, and phenacetin (Su et al., 2000; Bao et al., 2005; Fukami et al., 2006; Nakajima et al., 2006; Fukami et al., 2008). Despite their close identity, a difference of only 32 amino acids, CYP2A13 and CYP2A6 can metabolize the same substrate at different rates or with different metabolites. For example, although both CYP2A13 and CYP2A6 metabolize $AFB_1$, only CYP2A13 metabolizes $AFB_1$ to the carcinogenic/toxic epoxide metabolites (He et al., 2006). In the case of 4-aminobiphenyl, a major carcinogen found in tobacco smoke, and phenacetin, an analgesic and antipyretic withdrawn from the market after implication in human nephropathy, only CYP2A13 is efficient at metabolism while CYP2A6 either metabolizes these substrates at barely detectable rates or not at all (Flower, 1985; Fukami et al., 2006; Nakajima et al., 2006).

The overall structure of CYP2A13 is very similar to that of CYP2A6, but there are differences in the identity of ten amino acids surrounding the active site (Smith et al., 2007). These differences account for an active site in CYP2A13 which is 15-20% larger than the active site of CYP2A6 (Smith et al., 2007). The active site volume for CYP2A13 is reported at 307 $Å^3$, a volume intermediate to that of CYP2A6 (250 $Å^3$) and CYP1A2 (375 $Å^3$) (Sansen et al., 2007b; Smith et al., 2007). CYP2A13, CYP2A6, and CYP1A2 each have active sites that are planar, highly hydrophobic, and are lined with a number of aromatic phenylalanine residues. In these respects, the active sites are complimentary to their generally compact, aromatic substrates (Sansen et al., 2007b; Smith et al., 2007). Thus, the observed differences in substrate metabolism are likely due to a few amino acid side chains that differ between the CYP2A13 and CYP2A6 active sites rather than global structural differences.

We selected phenacetin as a substrate probe to determine which amino acids within the active site might be responsible for CYP2A substrate specificity because it has been extensively studied throughout the last twenty years (Fischbach and Lenk, 1985b; Fischbach and Lenk, 1985a). In order to determine the role that individual amino acids play in CYP2A phenacetin metabolic capability, a series of single and multiple mutants of CYP2A13 and CYP2A6 were examined in this study. Each resulting protein was examined for phenacetin binding ($K_D$) and the ability to catalyze phenacetin *O*-deethylation. Overall, these results identify four key amino acid residues that play a key role in determining the ability of CYP2A enzymes to metabolize phenacetin. To relate these functional findings to structural differences of the two active sites, we crystallized a CYP2A6 quadruple mutant containing all four key amino acids as a complex with phenacetin. This structure, combined with the known structures of CYP2A13 and CYP2A6, provides a structural rationale for the roles of the amino acids at positions 208, 300, 301, and 369 in controlling phenacetin metabolism by human CYP2A enzymes.

**Methods**

*Chemicals and Reagents*: Phenacetin and acetaminophen were purchased from Sigma-Aldrich (St. Louis, MO) at the highest purity available.

*Protein design, expression, and purification:* Rat NADPH cytochrome P450 oxidoreductase and cytochrome $b_5$ were expressed in *E. coli* and purified as described (Smith et al., 2007). The CYP2A13 and CYP2A6 proteins were engineered by truncating the N-terminal transmembrane sequence (Δ2-23), modifying the N-terminus, and adding four histidine residues to the C-terminus. These modifications were made to increase protein expression and facilitate purification as described previously (Smith et al., 2007). Mutations were produced using either pKK2A13dH or pKK2A6dH as a template and synthetic oligonucleotides (Genosys, Woodlands, TX) containing the desired nucleotide substitutions and selected silent mutations (Table 1) using the Quikchange® method (Stratagene, La Jolla, CA) (Schlicht et al., 2007). For construction of multiple mutants, the desired nucleotide changes were either incorporated simultaneously using one oligo if the changes were in close proximity (e.g. 300/301 and 365/366) or iteratively by adding an additional mutation to a template that already contained one or more mutations. All genes were completely sequenced to verify the desired mutation(s) and the absence of unintended mutations. The cytochrome P450 2A proteins were all expressed in *E. coli* TOPP-3 cells (Stratagene, La Jolla, CA) and purified as described previously (Smith et al., 2007).

The CYP2A6 I208S/I300F/G301A/G369S protein used for crystallography was purified as described, except that 1% ANAPOE-35 (Anatrace, Maumee, OH) was used instead of 4.8 mM Cymol-5 (Anatrace, Maumee, OH). This protein was additionally purified on a Superdex 200 16/60 gel filtration column (GE Healthcare, Uppasala, Sweden) in buffer A (50 mM KPi, pH 7.4, 20% glycerol, 0.5 M NaCl, and 1 mM EDTA). The eluting CYP2A6 I208S/I300F/G301A/G369S fractions were pooled and concentrated by centrifugal ultrafiltration with 5 mM phenacetin in buffer A. Detergent, 0.2% ANAPOE-X-405 (Anatrace, Maumee, OH), was added to the concentrated protein prior to crystallization.

*Reconstitution of Enzymes:* CYP2A13, CYP2A6, and mutants thereof were reconstituted with reductase and cytochrome $b_5$ for 20 minutes at room temperature before use. A 1:6:2 ratio of CYP450

enzymes to reductase to cytochrome $b_5$ was used for all metabolism experiments as this ratio gave maximal metabolism (*data not shown*).

*Phenacetin O-Deethylation:* The phenacetin O-deethylation metabolism assay procedure was modified from the method reported by Fukami and coworkers for use with purified CYP2A protein (Fukami et al., 2006). Reconstituted protein (30 pmol cytochrome P450, 180 pmol NADPH reductase, and 60 pmol cytochrome $b_5$) was added to 100 mM potassium phosphate buffer (pH 7.4) with phenacetin to a total volume of 300 µL. Single activity measurements were determined using a phenacetin concentration of 250 µM and a NADPH concentration of 500 µM. Kinetics were determined using phenacetin concentrations of 0-250 µM and an NADPH concentration of 1 mM. Reactions were initiated with the addition of NADPH and proceeded for 30 minutes while incubated in a water bath at 37ºC. Reactions were terminated with 15 µL 60% perchloric acid. Samples were centrifuged for five minutes at 5000 rpm and the supernatant removed for analysis by HPLC. HPLC analysis was accomplished using a 4.6 x 250 mm Phenomenex (Torrance, CA) Luna C18 column with a flow rate of 1 mL/min and an isocratic mobile phase consisting of 8% acetonitrile with 50 mM potassium phosphate solution (pH 4.9). Injected sample was monitored with UV absorption at 245 nm. Acetaminophen standards were prepared in the same manner as the samples except for the absence of the reconstituted protein system. Preliminary experiments showed that the absence of protein did not affect the standard curve (*data not shown*).

*Spectral Difference Assays:* Spectral difference assays were completed and analyzed as described by Schlicht *et al*. (Schlicht et al., 2007). Phenacetin concentrations ranged from 0.5 – 275 µM with measurements at $\geq$10 intervening concentrations.

*Protein Crystallization, Data Collection, and Structure Determination*: Crystals of 100 µM CYP2A6 I208S/I300F/G301A/G369S with 5 mM phenacetin were grown by hanging drop vapor diffusion. The protein was equilibrated against a 750 µL solution of 30% PEG 3350, 0.10 M Tris, pH 8.5, and 0.2 M Ammonium Sulfate. For data collection, crystals were flash cooled in liquid nitrogen after being immersed in a cryoprotectant consisting of 350 µL of synthetic mother liquor and 300 µL of 100% ethylene glycol. A native data set was collected at beamline 9-2 at the Stanford Synchrotron Radiation

Laboratory (Stanford, CA) using a 0.98 Å wavelength and temperature of 100 K. Data processing was completed using Mosflm (Leslie, 2006) and Scala (Evans, 2006). The CYP2A6 I208S/I300F/G301A/G369S mutant structure was solved by molecular replacement with the program PHASER (McCoy et al., 2007). The search model was CYP2A6 complexed with coumarin (PDB 1Z10, molecule B). Model building and refinement were done iteratively using COOT (Emsley and Cowtan, 2004) and REFMAC5 (Murshudov et al., 1997) in the CCP4 suite (1994). The final model exhibited an R value of 0.21 and $R_{free}$ value of 0.27 with four molecules in the asymmetric unit. Well defined electron density was present above the heme prosthetic group in molecules A, B and D of the asymmetric unit, but not in molecule C. Data collection and processing statistics are provided in Table 2.

*Structure Validation and Analysis*: The CYP2A6 I208S/I300F/G301A/G369S structure was validated using WHAT-IF (Vriend, 1990) and PROCHECK (Laskowski et al., 1993). The Ramachandran plot showed 90.7% of residues in the most favored regions, 8.6% in the additional allowed regions, 0.4% in the generously allowed regions, and 0.2% in the disallowed regions. Consistent with previous structures of CYP2A6, F42 was in the disallowed region for all four molecules, but was clearly defined in the $2|F_o|-|F_c|$ electron density map (Yano et al., 2005; Sansen et al., 2007a). Coordinates have been deposited in the Protein Data Bank (PDB code 3E6I). All voids used in structural analysis were calculated using VOIDOO (Kleywegt and Jones, 1994) with a probe radius of 1.4 Å and a grid mesh of 0.3 Å.

**Results**

*Phenacetin Dissociation Constants for CYP2A13, CYP2A6, and CYP2A13→2A6 Single Site Mutant Enzymes*: CYP2A13 and CYP2A6 had very different spectral responses upon addition of phenacetin. Titration of CYP2A13 with phenacetin yielded a classic type I spectral shift with a strong peak at 384 nm and trough at 419 nm, reflecting the iron transition from hexacoordinate low spin to pentacoordinate high spin (Figure 1A). The $K_D$ value for this binding was 34 μM. In contrast, at phenacetin concentrations up to 250 μM, CYP2A6 demonstrated very little spectral shift above the baseline noise level (Figure 1B), suggesting that either phenacetin did not bind or did not bind close enough in the active site to displace the water molecule present on the heme iron in the enzyme resting state.

Of the ten single substitutions made in CYP2A13, several types of alterations were observed in phenacetin binding affinity (Table 3). One mutant, the Leu to Ile substitution at position 366 (L366I), significantly increased binding affinity by a 15-fold decrease in $K_d$ to 2.2 μM. A second set of mutated proteins including L110V, A117V, and H372R had smaller effects on phenacetin binding, causing less than 2-fold decreases in the $K_D$ values. A third set of mutations including A213S, G369S, S208I, and M365V still yielded CYP2A13-like spectral shifts, but with 2- to 4-fold decreases in phenacetin affinity. In contrast, a fourth set of enzyme mutations at positions 300 and 301 demonstrated substantially reduced spectral responses to phenacetin titration. Titration of F300I with phenacetin reveals only a small trough at 420 nm, while titrations of CYP2A13 A301G had essentially no spectral shift (Figure 1C).

*Phenacetin O-deethylation Activity:* Initially, phenacetin *O*-deethylation activity was determined for all CYP2A enzymes at 250 μM phenacetin. This concentration was selected because it was ~25-times the $K_D$ for CYP2A13 in preliminary experiments (*data not shown*). At this concentration, CYP2A13 demonstrated an activity of ~3.4 pmol/min/pmol, while CYP2A6 had activity that was only 0.08 pmol/min/pmol, only barely above our lower limit of detection (Tables 4 and 5, respectively).

Of the ten CYP2A13 singly-substituted proteins, 5-fold and 3-fold increases in phenacetin *O*-deethylation were observed for A117V and L366I, respectively, while all other CYP2A13 mutations

resulted in markedly decreased phenacetin metabolism (Figure 2). The individual CYP2A13 mutations L110V, S208I, F300I, A301G, M365V, and G369S each reduced phenacetin metabolism to less than 15% of the wild type activity, with residues at positions 300, 301, 208, and 369 having the largest effects. The A213S and H372R mutations had much less dramatic effects on activity with rates ~1 pmol/min/pmol.

Most of the ten single CYP2A6 single mutants were similar to CYP2A6 in that they had little or no phenacetin *O*-deethylation activity (Figure 3). However, V110L, I300F, and S369G had low but significant levels of activity (0.2-0.3 pmol/min/mol) (Table 4). Since these results suggested that the ability of CYP2A13 to metabolize phenacetin must be the result of several additive differences in the human 2A active sites, multiple mutants at key positions identified by the binding and metabolism studies were generated and characterized. The doubly-mutated 2A6 protein V365M/I366L had almost no activity. However, the double mutant CYP2A6 I300F/G301A, had a moderate increase in activity to 0.6 pmol/min/pmol over either of the single mutants. Addition of the I208S or S369G substitutions to the 300/301 double mutant yielded further increases in phenacetin activity to 0.8 and 1.0 pmol/min/pmol, respectively (Table 4). The quadruple mutant CYP2A6 I300F/G301A/S369G/I208S had activity of 3 pmol/min/pmol, nearly equivalent to CYP2A13 wild type (Figure 3).

*Phenacetin Dissociation Constants for CYP2A6→2A13 Multiple Mutant Enzymes*:

Phenacetin dissociation constants were then determined for those CYP2A6 multiple mutant proteins that demonstrated significant phenacetin metabolism (Table 3). Like CYP2A6, the CYP2A6 G301A mutant protein gave essentially no spectral shift with phenacetin concentrations up to 250 μM. The single CYP2A6 I300F substitution however did have a slight spectral shift, but a reliable $K_D$ value could not be ascertained due to the very low absorption change. Combination of these mutations (I300F/G301A) yielded phenacetin binding with a high $K_D$ of 103 μM. Addition of I208S (I208S/I300F/G301A) decreased the $K_D$ to 63 μM. By comparison, addition of G369S to the I300F/G301A double mutant had a larger impact, reducing the $K_D$ to 13 μM, which is a greater affinity than that of wild type CYP2A13 ($K_D$ 35 μM). Combination of all four substitutions (I208S/I300F/G301A/G369S) yielded an intermediate $K_D$ of 21 μM (Figure 1D).

*Phenacetin O-deethylation Kinetic Parameters*: Kinetic parameters were subsequently determined for all proteins with phenacetin *O*-deethylation activity greater than 0.7 pmol/min/pmol in the single-concentration studies above. Additionally, because phenacetin has been used as a marker substrate for CYP1A2, the full-length version of this enzyme was also characterized alongside the CYP2A enzymes. CYP2A13 and CYP1A2 both had catalytic efficiencies of ~0.36 $\mu M^{-1}min^{-1}$ (Table 6). Despite their similar catalytic efficiencies, there was a marked difference in their kinetic parameters. CYP1A2 had a $k_{cat}$ of 9.68, three times greater than CYP2A13, but the $K_m$ of CYP1A2 was also about three times higher than the $K_m$ of CYP2A13 (Figure 4A).

Phenacetin metabolism by the CYP2A13 mutant enzymes varied considerably (Table 6). Two CYP2A13 mutations caused phenacetin metabolism at rates significantly higher than either CYP2A13 or CYP1A2. A117V has a 7.7-fold increase in $k_{cat}$ compared to CYP2A13 (Figure 4A). A concomitant 5-fold increase in $K_m$ resulted in a catalytic efficiency for the mutant that was 1.7-fold higher than CYP2A13. L366I had a $k_{cat}$ 3.6-fold higher than CYP2A13 (Figure 4A), but similar increases in $K_m$ yielded a catalytic efficiency similar to CYP2A13 (Table 6). A second set of CYP2A13 single mutants consisting of A213S, M365V, and H372R had decreases in $k_{cat}$ (Figure 4B) and catalytic efficiencies at or below that observed for CYP2A13 (Table 6).

Although the phenacetin *O*-deethylation activity for all of the 2A6 single mutants were too low to determine reliable kinetic parameters, several of the multiple mutants had significant activity, thus permitting kinetic analysis (Table 6). The CYP2A6 triple mutants I300F/G301A/I208S and I300F/G301A/S369G both had $k_{cat}$ values of ~0.9 pmol/min/pmol, which was significantly increased from CYP2A6 and ~1/3 of that observed for CYP2A13 (Figure 4C). However, the $K_m$ for the triple mutant CYP2A6 I300F/G301A/S369G was 4.9 μM or about half of CYP2A13, while the triple mutant CYP2A6 I300F/G301A/I208S had a $K_m$ of 38.9 μM or 3.6 times higher than CYP2A13 (Table 6). As a result, the catalytic efficiency of I208S/I300F/G301A was the lowest observed, while I300F/G301A/S369G was almost half that of CYP2A13. Finally, the quadruple mutant CYP2A6 I208S/I300F/G301A/S369G had

catalytic efficiency very similar to CYP2A13, as a result of an almost identical $K_m$ and a $k_{cat}$ only slightly lower than CYP2A13 (Figure 4C).

*Structure of 2A6 I208S/I300F/G301A/S369G with Phenacetin:* Although analysis of the wild type enzyme structures and docking studies suggested that the ability of these mutations to interconvert phenacetin activity were primarily due to a relief of steric clashes in the active site near F300, the phenacetin-complexed structure of the CYP2A6 I208S/I300F/G301A/G369S mutant was determined to further evaluate this idea. The overall tertiary structure of the CYP2A6 quadruple mutant was very similar to both wild type CYP2A6 and CYP2A13 with root mean squared deviations (r.m.s.d.) of the Cα atoms of 0.39 and 0.47 Å, respectively. This was similar to the r.m.s.d. between the four molecules of the CYP2A6 quadruple mutant asymmetric unit (0.29 to 0.48 Å). The greatest variation in tertiary structure was observed in the solvent exposed loops.

All four mutations were clearly evident in the active site. Furthermore, electron density that corresponded to phenacetin was present in three of the four protein molecules. This density indicated phenacetin oriented with the acetamide directed toward residue 300 and the ethoxy group oriented toward the heme iron, consistent with the experimentally observed *O*-deethylation (Figure 5A). Phenacetin appears to have some flexibility in orientation as the molecule varied somewhat between all three molecules, in terms of the plane of the phenyl ring and the flexible ethoxy tail (Figure 5B). In each molecule, however, there is a conserved hydrogen bond (2.9-3.14 Å) between N297 and the amide oxygen of phenacetin and the distance from the subterminal carbon and the iron was 4-4.5 Å.

The orientation of the L370 side chain also varied between molecules. Molecule A and C had the leucine side chain oriented so that it is rotated away from the phenacetin (Figure 5B). In molecule A, the terminal carbon of phenacetin ethoxy chain projects toward this side chain and the repositioning of L370 makes additional space available to the ligand. This side chain had previously been noted to have an alternate conformation in molecule A of the CYP2A6 structure complexed with coumarin (PDB 1Z10) (Yano et al., 2005). Due to the rotation of L370 away from the active site, the active site volumes for molecules A and C are 300 $Å^3$ and 297 $Å^3$, respectively. In contrast, the active site volume is reduced in

molecules B (270 $Å^3$) and D (272 $Å^3$) (Figure 5C). Replacement of the adjacent S369 by the glycine present in CYP2A13 may result in additional flexibility for L370.

The mutated side chains F300 and A301 were located in the same orientation in all four molecules. F300 forms the top portion of the active site while A301 forms part of the side (Figure 5B). The S208 side chain is rotated toward the active site in molecule A, while in molecules B, C, and D it is angled away from the active site (Figure 5B). The rotation of this side chain does not appear to affect the active site volume.

The active site of the quadruple mutant is primarily hydrophobic, with residue N297 as the most orientating feature. Despite the small active site volume, phenacetin has some degree of flexibility within the active site, as indicated by its different orientation in the three molecules.

**Discussion**

Experimental analysis of phenacetin binding and metabolism by human CYP2A enzymes together with the structure of the CYP2A6 I208S/I300F/G301A/G369S mutant provide insights into the substrate specificity of the human cytochrome P450 2A family. The quadruple mutant is able to metabolize phenacetin with a $K_m$ nearly identical to CYP2A13 and a $k_{cat}$ ~75% of CYP2A13. The ability to create phenacetin metabolism in CYP2A6 where essentially none existed previously demonstrates that these four residues largely control the ability to bind and metabolize phenacetin in human 2A enzymes. To further understand the contributions of these four residues, the structure of the quadruple CYP2A6 mutant was determined in complex with phenacetin.

Comparisons of the CYP2A13, CYP2A6, and the CYP2A6 I208S/I300F/G301A/G369S active sites give insight into how these four mutations significantly alter CYP2A functionality (Figure 6). CYP2A6 has one of the smallest human P450 active sites, with a volume of 214-230 $Å^3$ for the four CYP2A6 molecules (PDB 1Z10). CYP2A13 has a larger active site, with a volume of ~304 $Å^3$ (PDB 2P85). All of the quadruple mutant molecules had intermediate volumes from 270 – 300 $Å^3$, depending primarily on the L370 conformation.

The residues 300 and 301 appear to play the most critical roles in phenacetin binding and metabolism, consistent with their close interaction with phenacetin in the crystal structure. The phenylalanine at position 300 is torsioned away from ligand in CYP2A13 and the quadruple mutant, resulting in additional active site space in this region to accommodate the phenacetin acetamide. Substitution of the phenylalanine to the smaller isoleucine in CYP2A6 actually causes a decrease in active site space available to the ligand because the isoleucine side chain projects directly into the active site. Of particular note is a steric clash between CYP2A6 I300 and the terminal carbon of the amide end of phenacetin, which is particularly evident when viewing the active site cavities (Figure 7). Functional effects have also been observed for a CYP2A6 I300V mutation in a random mutagenesis screen for increased indole metabolism (Wu et al., 2005). At position 301, alanine appears to be essential for CYP2A phenacetin binding and metabolism. The methyl side chain of alanine is directed toward the face

of phenacetin just proximal to the ring. Substitution to glycine may remove packing interactions needed to stabilize the phenacetin in the active site. This residue has not previously been identified as altering CYP2A function.

The third mutated residue essential for phenacetin metabolism is residue 208. In CYP2A13 and the quadruple mutant, this residue is a serine and located in helix F directly above residue 300. In addition to the reduction in side chain size compared to the isoleucine found in CYP2A6, S208 is torsioned away from the active site in the majority of the quadruple mutant molecules. This creates space that likely facilitates torsion of F300 away from the active site, indirectly increasing space for phenacetin binding as described above. Additionally, the residue at position 208 effects the orientation of the adjacent conserved F209 (Figure 6). The orientation of F209 away from phenacetin in the quadruple mutant is identical to the position of F209 in CYP2A13 and also creates active site volume that would better accommodate phenacetin (Figure 7). The CYP2A13 mutation S208I was previously shown to alter metabolism of the nicotine-derived procarcinogen NNK (He et al., 2004a). Mutation at position 209 has also been shown to alter the specificity of mouse CYP2A enzymes (Negishi et al., 1996).

The fourth residue, 369, is located on the opposite side of the active site cavity and somewhat more distant from the phenacetin molecule. The serine found at this position in CYP2A6 is oriented toward the proximal side of the heme, where it interacts with the heme propionate (Figure 6). In CYP2A13 and the quadruple mutant a glycine is found at this position and the contact with the heme propionate is instead mediated by a water molecule stabilized via interaction with the protein backbone. Instead, the residue at position 369 may play an indirect role in phenacetin binding by modulating the position of the adjacent L370 residue. In all six molecules of CYP2A13, L370 is positioned with its side chain is oriented alongside the active site cavity. In the 1Z10 structure of CYP2A6, three of the four of the molecules have L370 directed into the active site cavity, reducing the volume available to ligands (Figure 6). However, one of the four CYP2A6 molecules was modeled with two alternate conformations, 50% occupancy extending into the active site like the remaining CYP2A6 molecules and 50% occupancy oriented alongside the active site as in CYP2A13. In the CYP2A6 quadruple mutant structure, two of the four

molecules have the L370 side chain in the CYP2A13 position and in the other two molecules L370 is in the CYP2A6-dominant orientation. Thus, additional flexibility imparted when glycine is at 369 may facilitate movement of L370 so that it is more likely to be positioned alongside the cavity as seen in CYP2A13. The added flexibility of L370 to adopt this second conformation would result in more active site space available to ligands and likely contributes to increased phenacetin binding and metabolism.

The CYP2A6 I208S/I300F/G301A/G369S crystal structure also gives structural insight into the two CYP2A13 mutations that resulted in increases in phenacetin $k_{cat}$ substantially above that of the CYP2A13 wild type enzyme. The first, CYP2A13 A117V, had a 40% decrease in $K_D$, a 4.5-fold increase in $K_m$, and an overall two-fold increase in catalytic efficiency, suggesting multiple effects in binding and catalysis. The CYP2A13 A117V mutation has been previously shown to be important for coumarin and NNK metabolism (He et al., 2004b). Although the quadruple mutant's valine side chain projects further into the active site toward the phenacetin than the CYP2A13 alanine, the reduction in volume in this portion of the active site complements and may be beneficial in orientating the phenacetin within the active site (Figure 7). The L366I mutation had an overall catalytic efficiency similar to wild type CYP2A13, with ~3.5-fold increases in both $K_m$ and $V_{max}$. However, this mutation also dramatically increased binding affinity. The CYP2A13 L366I mutation is located close to residues 365 and 369 near the alkyl chain of phenacetin. Mutation from the leucine found in CYP2A13 to the isoleucine in CYP2A6 would also likely increase the size of the active site cavity.

CYP2A13 L110V and M365V also reduced the phenacetin *O*-deethylation activity at 250 µM to less than 15% of the wild type CYP2A13 enzyme. These mutations were not incorporated into the multiple mutant series because the quadruple mutant substitutions were sufficient to closely approximate the kinetic parameters observed for the CYP2A13 enzyme. In CYP2A13, the M365 side chain extends into the active site next to L366, while in CYP2A6 the shorter valine side chain at this position does not actually form part of the active site as the side chain of I366 extends further and shields V366 from the active site (Figure 6). It is possible that the CYP2A13 M365V mutant exhibits a loss in activity because an increase in active site volume in this region is not conducive to phenacetin stabilization in the active

site. In contrast, the L366I substitution results in a beneficial effect on binding and metabolism. It seems likely that the structural results of mutations at adjacent residues 365 and 366 may be related as their mutation in CYP2A13 resulted in opposing effects. The effect of the CYP2A13 L110V mutation is more difficult to explain. This residue is not located in the active site; instead it is located in the B′ helix across from residue 208. Furthermore, although the CYP2A13 L110V mutant has a significant reduction in phenacetin metabolism activity, it causes a small increase (less than 2-fold) in phenacetin binding affinity. Further investigation will be needed to determine why this mutation causes such a striking reduction in phenacetin *O*-deethylation.

The crystal structure of CYP2A6 I208S/I300F/G301A/G369S together with the phenacetin binding and metabolism data clearly indicates that the ability of CYP2A13 to metabolize phenacetin is the aggregate result of several differences from the CYP2A6 the active site. This is why incorporation of individual 2A13 residues into CYP2A6 at all ten active site positions where the parent enzymes differ yielded no difference or only small increases in phenacetin metabolism. Changes in phenacetin metabolism were observed with the multiple mutants, which is consistent with the fact that multiple residue alterations are necessary for phenacetin to bind in CYP2A6. The two 2A6 triple mutant proteins (2A6 I208S/I300F/G301A and 2A6 I300F/G301A/S369G) had significant phenacetin metabolic activity ($k_{cat}$ ~1 $min^{-1}$) indicating that increasing the active site volume around residue 300 and either 370 or 209 permits enough volume for phenacetin to bind albeit not as well as in CYP2A13. The quadruple mutant (2A6 I208S/I300F/G301A/S369G) has phenacetin metabolism parameters nearly identical to those of CYP2A13 as well as an active site volume substantially larger than CYP2A6. The active site of this quadruple mutant closely resembles that of CYP2A13. Some of the CYP2A6 residues (V117 and I366) are actually beneficial to phenacetin metabolism and may be reflected in the quadruple mutant's slightly increased binding affinity, $K_D$ 21 μM, as compared to a $K_D$ of 34 μM in CYP2A13. The ability to create phenacetin metabolism in CYP2A6 where essentially none existed previously demonstrates that these four residues largely control the ability to bind and metabolize phenacetin in human 2A enzymes.

In conclusion, this study identifies four amino acid residues, 208, 300, 301, and 369, that are responsible for controlling the metabolism of phenacetin in the human cytochrome 2A family. The crystal structure of CYP2A6 I208S/I300F/G301A/S369G and comparison to the active sites of CYP2A13 and CYP2A6 suggests that the ability of CYP2A enzymes to metabolize phenacetin is largely the culmination of steric effects of the substituted side chains themselves and their effects on the positions of adjacent side chains F209 and L370. Though phenacetin is no longer used clinically as an analgesic, it was used in these studies as a model substrate due to the difference in affinity between CYP2A6 and CYP2A13. Further investigations will determine whether these same residues are responsible for differences in selectivity for other CYP2A ligands like the procarcinogen NNK.

**Acknowledgements**

Thanks are due to Jenny Morrison, Chad Schroeder, and Melanie Blevins for construction of the CYP2A13 mutants and to Linda Blake, Naseem Nikaeen, Matthew Axtman, Agnes Walsh, and Kyle Bailey for construction of the CYP2A6 mutants. Thanks are also due to Christopher Wood for his assistance in expressing and purifying some of the CYP2A13 mutants. Full length human CYP1A2 was a generous gift from Dr. Fred Guengerich (Vanderbilt University School of Medicine, Nashville, TN). Thanks are given to Linda Blake for critical reading of the manuscript. Crystals were grown and initially screened using the facilities of the Protein Structure Laboratory core facility at The University of Kansas. We would like to acknowledge access to the facilities and excellent support staff of SSRL. The SSRL is operated by the Department of Energy, Office of Basic Energy Sciences. The SSRL Biotechnology Program is supported by the National Institutes of Health, National Center for Research Resources, Biomedical Technology Program, and by the Department of Energy, Office of Biological and Environmental Research.

**References**

(1994) The CCP4 suite: programs for protein crystallography. *Acta Crystallogr D Biol Crystallogr* **50:**760-763.

Bao Z, He XY, Ding X, Prabhu S and Hong JY (2005) Metabolism of nicotine and cotinine by human cytochrome P450 2A13. *Drug Metab Dispos* **33:**258-261.

DeLano WL (2002) The PyMOL Molecular Graphics System, DeLano Scientific, Palo Alto, CA.

Emsley P and Cowtan K (2004) Coot: model-building tools for molecular graphics. *Acta Crystallogr D Biol Crystallogr* **60:**2126-2132.

Evans P (2006) Scaling and assessment of data quality. *Acta Crystallogr D Biol Crystallogr* **62:**72-82.

Fischbach T and Lenk W (1985a) Additional routes in the metabolism of phenacetin. *Xenobiotica* **15:**149-164.

Fischbach T and Lenk W (1985b) The metabolism of N-hydroxyphenacetin in vitro and in vivo. *Xenobiotica* **15:**915-927.

Flower RJ, S. Moncada, and J.R. Vane (1985) Analgesic-antipyretics and anti-inflammatory agents, in: *Goodman and Gilman's The Pharmacological Basis of Therapeutics* (A.G. Gilman LSG, T.W. Rall, and G. Murad ed), pp 674-715, Macmillan Publishing Co., New York.

Fukami T, Katoh M, Yamazaki H, Yokoi T and Nakajima M (2008) Human Cytochrome P450 2A13 Efficiently Metabolizes Chemicals in Air Pollutants: Naphthalene, Styrene, and Toluene. *Chem Res Toxicol* **21:**720-725.

Fukami T, Nakajima M, Sakai H, Katoh M and Yokoi T (2006) CYP2A13 metabolizes human CYP1A2 substrates, phenacetin and theophilline. *Drug Metab Dispos.*

He XY, Shen J, Ding X, Lu AY and Hong JY (2004a) Identification of critical amino acid residues of human metabolic activation of 4-(methylnitrosamino)-1-(3-pyridyl)-1-tobacco-specific carcinogen. *Drug Metab Dispos* **32:**1516-1521.

He XY, Shen J, Hu WY, Ding X, Lu AY and Hong JY (2004b) Identification of Val117 and Arg372 as critical amino acid residues for the activity difference between human CYP2A6 and CYP2A13 in coumarin 7-hydroxylation. *Arch Biochem Biophys* **427:**143-153.

He XY, Tang L, Wang SL, Cai QS, Wang JS and Hong JY (2006) Efficient activation of aflatoxin B1 by cytochrome P450 2A13, an enzyme predominantly expressed in human respiratory tract. *Int J Cancer* **118:**2665-2671.

Kleywegt GJ and Jones TA (1994) Detection, delineation, measurement and display of cavities in macromolecular structures. *Acta Crystallogr D Biol Crystallogr* **50:**178-185.

Laskowski RA, MacArthur MW, Moss DS and Thornton JM (1993) PROCHECK: a program to check the stereochemical quality of protein structures. *Journal of Applied Crystallography* **26:**283-291.

Leslie AG (2006) The integration of macromolecular diffraction data. *Acta Crystallogr D Biol Crystallogr* **62:**48-57.

McCoy AJ, Grosse-Kunstleve RW, Adams PD, Winn MD, Storoni LC and Read RJ (2007) Phaser crystallographic software. *Journal of Applied Crystallography* **40:**658-674.

Murshudov GN, Vagin AA and Dodson EJ (1997) Refinement of macromolecular structures by the maximum-likelihood method. *Acta Crystallogr D Biol Crystallogr* **53:**240-255.

Nakajima M, Itoh M, Sakai H, Fukami T, Katoh M, Yamazaki H, Kadlubarz FF, Imaoka S, Funae Y and Yokoi T (2006) CYP2A13 expressed in human bladder metabolically activates 4-aminobiphenyl. *International Journal of Cancer* **119:**2520-2526.

Negishi M, Uno T, Honkakoski P, Sueyoshi T, Darden TA and Pedersen LP (1996) The roles of individual amino acids in altering substrate specificity of the P450 2a4/2a5 enzymes. *Biochimie* **78:**685-694.

Sansen S, Hsu MH, Stout CD and Johnson EF (2007a) Structural insight into the altered substrate specificity of human cytochrome P450 2A6 mutants. *Arch Biochem Biophys* **464:**197-206.

Sansen S, Yano JK, Reynald RL, Schoch GA, Griffin KJ, Stout CD and Johnson EF (2007b) Adaptations for the Oxidation of Polycyclic Aromatic Hydrocarbons Exhibited by the Structure of Human P450 1A2. *J Biol Chem* **282:**14348-14355.

Schlicht KE, Michno N, Smith BD, Scott EE and Murphy SE (2007) Functional characterization of CYP2A13 polymorphisms. *Xenobiotica***:**1-11.

Smith BD, Sanders JL, Porubsky PR, Lushington GH, Stout CD and Scott EE (2007) Structure of the human lung cytochrome P450 2A13. *J Biol Chem*.

Su T, Bao ZP, Zhang QY, Smith TJ, Hong JY and Ding XX (2000) Human cytochrome p450 CYP2A13: Predominant expression in the respiratory tract and its high efficiency metabolic activation of a tobacco-specific carcinogen, 4-(methylnitrosamino)-1-(3-pyridyl)-1-butanone. *Cancer Research* **60:**5074-5079.

Vriend G (1990) WHAT IF: a molecular modeling and drug design program. *J Mol Graph* **8:**52-56, 29.

Wu ZL, Podust LM and Guengerich FP (2005) Expansion of substrate specificity of cytochrome P450 2A6 by random and site-directed mutagenesis. *J Biol Chem* **280:**41090-41100.

Yano JK, Hsu MH, Griffin KJ, Stout CD and Johnson EF (2005) Structures of human microsomal cytochrome P450 2A6 complexed with coumarin and methoxsalen. *Nat Struct Mol Biol* **12:**822-823.

Zhang JY, Wang Y and Prakash C (2006) Xenobiotic-metabolizing enzymes in human lung. *Curr Drug Metab* **7:**939-948.

**Footnotes**

This work was supported by the NIH grant GM076343 (EES). Portions of this work were presented in a meeting abstract at Experimental Biology 2008.

**Reprint request to:** Emily Scott, Ph.D., Department of Medicinal Chemistry, University of Kansas, 1251 Wescoe Hall Dr., Lawrence, KS 66045, eescott@ku.edu

**Figure Legends**

Figure 1. Spectral changes upon phenacetin binding to (A) CYP2A13, (B) CYP2A6, (C) CYP2A13 A301G, and (D) CYP2A6 I208S/I300F/G301A/S369G. Increasing concentrations of phenacetin during the titrations are indicated by spectra scans colored from red (low concentration 0.5 μM) to indigo (high concentration 250-300 μM).

Figure 2. Effects of mutation on phenacetin *O*-deethylation rates by CYP2A13 mutant proteins.

Figure 3. Effects of mutation on phenacetin *O*-deethylation rates by CYP2A6 mutant proteins.

Figure 4. Phenacetin metabolism by CYP1A2, CYP2A13, and CYP2A13 mutant proteins. Data represents a global fit to two independent experiments with each point performed in triplicate.

Figure 5. The CYP2A6 I208S/I300F/G301A/G369S structure. A. Electron density surrounding the phenacetin ligand found in molecule B of the CYP2A6 I208S/I300F/G301A/G369S structure. B. Structural overlay of the four non-identical molecules found in the CYP2A6 I208S/I300F/G301A/G369S asymmetric unit, highlighting the differences in phenacetin and L370 positions. Molecules A (green), B (yellow), and D (blue) contain one molecule of phenacetin, while molecule C (pink) did not have electron density for phenacetin. D. Active site volume comparison between molecule A (green mesh, 300 $Å^3$) and molecule B (yellow mesh, 270 $Å^3$). The difference in active site volume among the four CYP2A6 quadruply-mutated protein molecules appears to depend largely on the position of L370. All structure figures were made with Pymol (DeLano, 2002). Hydrogen bonding to N297 is indicated by black dashed lines.

Figure 6. Comparison of the active sites of CYP2A6 (purple, PDB 1Z10, molecule B), CYP2A6 I208S/I300F/G301A/G369S with phenacetin (green, molecule A), and CYP2A13 (orange, PDB 2P85, molecule A). The four residues mutated in the CYP2A6 quadruple mutant, identical to the residues found in CYP2A13, are labeled in bold. The hydrogen bond from phenacetin to N297 is shown as a dashed black line.

Figure 7. Stereo view comparison of the active site cavities of CYP2A6 (purple protein and mesh, PDB 1Z10), CYP2A13 (orange protein and mesh, PDB 2P85), and CYP2A6 I208S/I300F/G301A/G369S

(green protein and mesh). Steric clashes between the phenacetin and CYP2A6 residues 300, 209, and 370 are evident.

DMD Fast Forward. Published on September 8, 2008 as DOI: 10.1124/dmd.108.023770
This article has not been copyedited and formatted. The final version may differ from this version.



**Tables**

Table 1. Sequences are shown below for one of two complementary oligonucleotides used in the construction of the indicated mutation(s). Bold indicates changes from the wild type sequence. Underline indicates the location of the desired mutation. Italics indicate additional synonymous changes that alter a restriction site and were used to facilitate identification of plasmids containing the desired nonsynonymous mutation. Multiple mutations were made by sequential addition of changes using these same oligonucleotides.

| CYP2A6 Mutation | Sequence (5' to 3') | Restriction Site Altered |
|---|---|---|
| V110L | GCC ACC TTC GAC TGG **C**T**G** TT***T*** AAA GGC TAT GGC | add DraI |
| V117A | GGC TAT GGC GTG G**C**A TTC AGC AAC GGG | add BbsI |
| I208S | GC ATG ATG CTA GGA A***G***C TTC CAG TTC ACG TCA ACC TCC | delete HindIII |
| S213A | GGA ATC TTC CAG TTC ACG **G**C**G** AC***G*** TCC ACG GGG CAG C | add AatII |
| I300F | CG TTG AAC CTC TTC **A**T**C** GGG GG***T*** AC***T*** GAG ACC GTG AGC | add KpnI |
| G301A | CG TTG AAC CTC TTC ATT G**C**G GG***T*** AC***C*** GAG ACC GTC AGC | add KpnI |
| V365M | CAA AGA TTT GGA GAC **A**TG ATC CCC ATG AGT TTG | none |
| I366L | C CAA AGA TTT GGA GAC GT***C*** **C**T**G** CCC ATG AGT TTG GCC C | add AatII |
| S369G | C GTG ATC CCC ATG **G**GT TTG G*C*C CGC AGA GTC AAA AAG G | delete NcoI |
| R372H | CCC ATG AGT TTG GCC C**A**C AGA GT***G*** AAA AAG GAC ACC | delete DraIII |
| I300F/G301A | CC ACG TTG AAC CTC TTC **T**T**C** G**C**G GG***T*** AC***C*** GAG ACC GTC AGC ACC | add KpnI |
| V365M/I366L | CAA AGA TTT GGA GAC **A**TG **C**T**G** CCC ATG AGT TTG GCC CGC | none |

DMD Fast Forward. Published on September 8, 2008 as DOI: 10.1124/dmd.108.023770
This article has not been copyedited and formatted. The final version may differ from this version.



Table 2. Data collection and refinement statistics.

| | CYP2A6 I208S/I300F/G301A/S369G with Phenacetin |
|---|---|
| **Data collection** | |
| Space group | $P2_1$ |
| Cell dimensions | |
| a, b, c (Å) | 70.84, 159.13, 103.99 |
| α, β, γ (°) | 90.0, 92.08, 90.0 |
| Resolution[a] (Å) | 87.04 - 2.15 (2.21 - 2.15) |
| Total observations[a] | 270986 (19484) |
| Unique reflections[a] | 121786 (8964) |
| Completeness[a] (%) | 97.8 (97.5) |
| $R_{sym}$[a,b] | 0.059 (0.357) |
| $I/\sigma I$[a] | 10.5 (1.6) |
| **Refinement** | |
| Resolution (Å) | 87.04 - 2.15 |
| No. reflections | 115652 |
| $R/R_{free}$ (%) | 21.1/26.9 |
| No. atoms | |
| Protein | 15029 |
| Ligand | 39 |
| Heme | 172 |
| Water | 297 |
| B-factors | |
| Protein | 39.2 |
| Ligand | 66.6 |
| Heme | 27.2 |
| Water | 35.4 |
| Rms. deviations | |
| Bond lengths (Å) | 0.014 |
| Bond angles (°) | 1.5 |

[a] Values in parentheses are for highest-resolution shell.

[b] $R_{sym} = \Sigma_{hkl}\Sigma_i \left| I_i(hkl) - \langle I(hkl) \rangle \right| / \Sigma_{hkl}\Sigma_i I_i(hkl)$

DMD Fast Forward. Published on September 8, 2008 as DOI: 10.1124/dmd.108.023770
This article has not been copyedited and formatted. The final version may differ from this version.



Table 3. Phenacetin dissociation constants ($K_D$).

| Protein | $K_D$ (μM) | $\frac{K_D(\text{mutant})}{K_D(\text{2A13wt})}$ |
|---|---|---|
| 2A13* | 34 | 1.0 |
| L110V | 18 | 0.5 |
| A117V | 20 | 0.6 |
| S208I | 108 | 3.1 |
| A213S | 65 | 1.9 |
| F300I | N.A.[a] | N.A.[a] |
| A301G | N.A.[a] | N.A.[a] |
| M365V | 135 | 4.0 |
| L366I | 2.2 | 0.1 |
| G369S | 97 | 2.9 |
| H372R | 20. | 0.6 |
| 2A6 | N.A.[a] | N.A.[a] |
| I300F/G301A | 103 | 3.0 |
| I208S/I300G/G301A | 63 | 1.8 |
| I300F/G301A/G369S | 13 | 0.4 |
| I208S/I300F/G301A/G369S | 21 | 0.6 |

[a] N.A. Only a reduced spectral shift was detected, which did not allow determination of $K_D$. Details of titration given in text and Figure 1.

*$K_D$ value represents the mean of three independent trials.

DMD Fast Forward. Published on September 8, 2008 as DOI: 10.1124/dmd.108.023770
This article has not been copyedited and formatted. The final version may differ from this version.



Table 4. Phenacetin *O*-deethylation rates and comparisons for CYP2A13, and mutations thereof. All assays used 250 μM phenacetin.

| Protein | Rate of product formation (pmol/min/pmol)[a] | $\frac{Activity_{mutant}}{Activity_{CYP2A13}}$ |
|---|---|---|
| CYP2A13 | 3.39 ± 0.55 | 1.00 |
| L110V | 0.40 ± 0.07 | 0.12 |
| A117V | 17.84 ± 1.91 | 5.26 |
| S208I | 0.35 ± 0.06 | 0.10 |
| A213S | 1.48 ± 0.50 | 0.44 |
| F300I | 0.07 ±0.01 | 0.02 |
| A301G | 0.18 ± 0.03 | 0.05 |
| M365V | 0.49 ± 0.11 | 0.14 |
| L366I | 11.41 ± 1.24 | 3.37 |
| G369S | 0.36 ± 0.12 | 0.11 |
| H372R | 1.06 ± 0.04 | 0.31 |

[a] Data represent the average of two independent experiments each conducted in triplicate.

DMD Fast Forward. Published on September 8, 2008 as DOI: 10.1124/dmd.108.023770
This article has not been copyedited and formatted. The final version may differ from this version.



Table 5. Phenacetin *O*-deethylation rates and comparisons for CYP2A6, and mutations thereof. All assays used 250 μM phenacetin.

| Protein | Rate of product formation (pmol/min/pmol)[a] | $\frac{Activity_{mutant}}{Activity_{CYP2A6}}$ |
|---|---|---|
| 2A6 | 0.08 ± 0.04 | 1.00 |
| V110L | 0.31 ± 0.11 | 3.90 |
| V117A | < det. lim.[b] | N.A.[c] |
| I208S | < det. lim.[b] | N.A.[c] |
| S213A | 0.08 ± 0.00 | 0.95 |
| I300F | 0.21 ± 0.04 | 2.66 |
| G301A | 0.07 ± 0.01 | 0.84 |
| V365M | 0.13 ± 0.03 | 1.69 |
| I366L | < det. lim.[b] | N.A.[c] |
| S369G | 0.21 ± 0.05 | 2.59 |
| R372H | 0.14 ± 0.09 | 1.73 |
| V365M/I366L | 0.12 ± 0.04 | 1.50 |
| I300F/G301A | 0.63 ± 0.09 | 7.85 |
| I208S/I300F/G301A | 0.81 ± 0.12 | 10.17 |
| I300F/G301A/S369G | 1.02 ± 0.09 | 12.86 |
| I208S/I300F/G301A/S369G | 3.03 ± 0.29 | 38.08 |

[a] Data represent the average of two independent experiments each conducted in triplicate.

[b] Value below the detection limit of our system (0.026 pmol/min/pmol).

[c] Not applicable.

DMD Fast Forward. Published on September 8, 2008 as DOI: 10.1124/dmd.108.023770
This article has not been copyedited and formatted. The final version may differ from this version.



Table 6. Kinetic Parameters for CYP1A2, CYP2A13, and mutants of CYP2A13 and CYP2A6[a].

| Enzyme | $K_m$ (μM) | $k_{cat}$ ($min^{-1}$) | $k_{cat}/K_m$ ($\mu M^{-1}min^{-1}$) | $\frac{(k_{cat}/K_m)_{mutant}}{(k_{cat}/K_m)_{2A13}}$ |
|---|---|---|---|---|
| 1A2[b] | 27.3 ± 2.2 | 9.68 ± 0.25 | 0.36 | 0.94 |
| 2A13 | 10.7 ± 2.0 | 3.82 ± 0.14 | 0.36 | 1.0 |
| A117V | 47.8 ± 5.8 | 29.4 ± 1.19 | 0.62 | 1.7 |
| A213S | 20.6 ± 2.5 | 2.14 ± 0.06 | 0.10 | 0.29 |
| M365V | 20.4 ± 4.7 | 0.93 ± 0.05 | 0.05 | 0.12 |
| L366I | 36.3 ± 4.5 | 13.7 ± 0.6 | 0.38 | 1.05 |
| H372R | 4.8 ± 1.3 | 1.91 ± 0.06 | 0.40 | 1.02 |
| 2A6 | N.D.[c] | N.D.[c] | N.D.[c] | N.D.[c] |
| I208S/I300F/G301A | 38.9 ± 7.0 | 0.98 ± 0.06 | 0.03 | 0.07 |
| I300F/G301A/S369G | 4.9 ± 0.5 | 0.89 ± 0.01 | 0.18 | 0.52 |
| I208S/I300F/G301A/G369S | 10.3 ± 0.8 | 2.88 ± 0.04 | 0.28 | 0.75 |

[a] Data represent the average of two independent experiments each with all concentrations conducted in triplicate.

[b] This is the full length enzyme.

[c] N.D., Reliable kinetic values could not be determined with enzyme with activities <0.7 pmol/min/mol at 250 μM phenacetin (Tables 2 and 3).

Figure 1

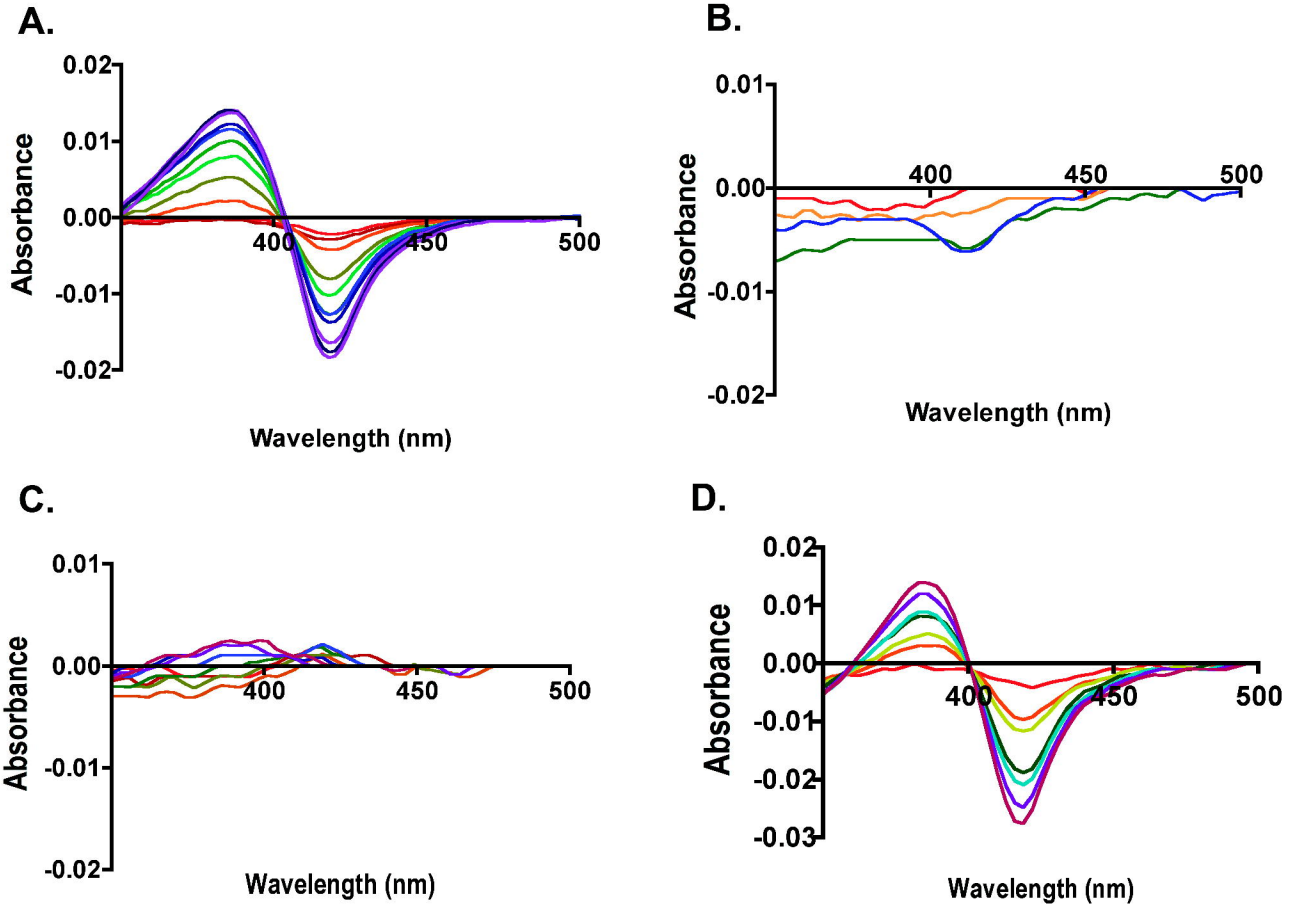
A.
0.02
0.01
0.00
-0.01
-0.02
Absorbance
400
450
500
Wavelength (nm)
B.
0.01
0.00
-0.01
-0.02
Absorbance
400
450
500
Wavelength (nm)
C.
0.01
0.00
-0.01
-0.02
Absorbance
400
450
500
Wavelength (nm)
D.
0.02
0.01
0.00
-0.01
-0.02
-0.03
Absorbance
400
450
500
Wavelength (nm)

Figure 2

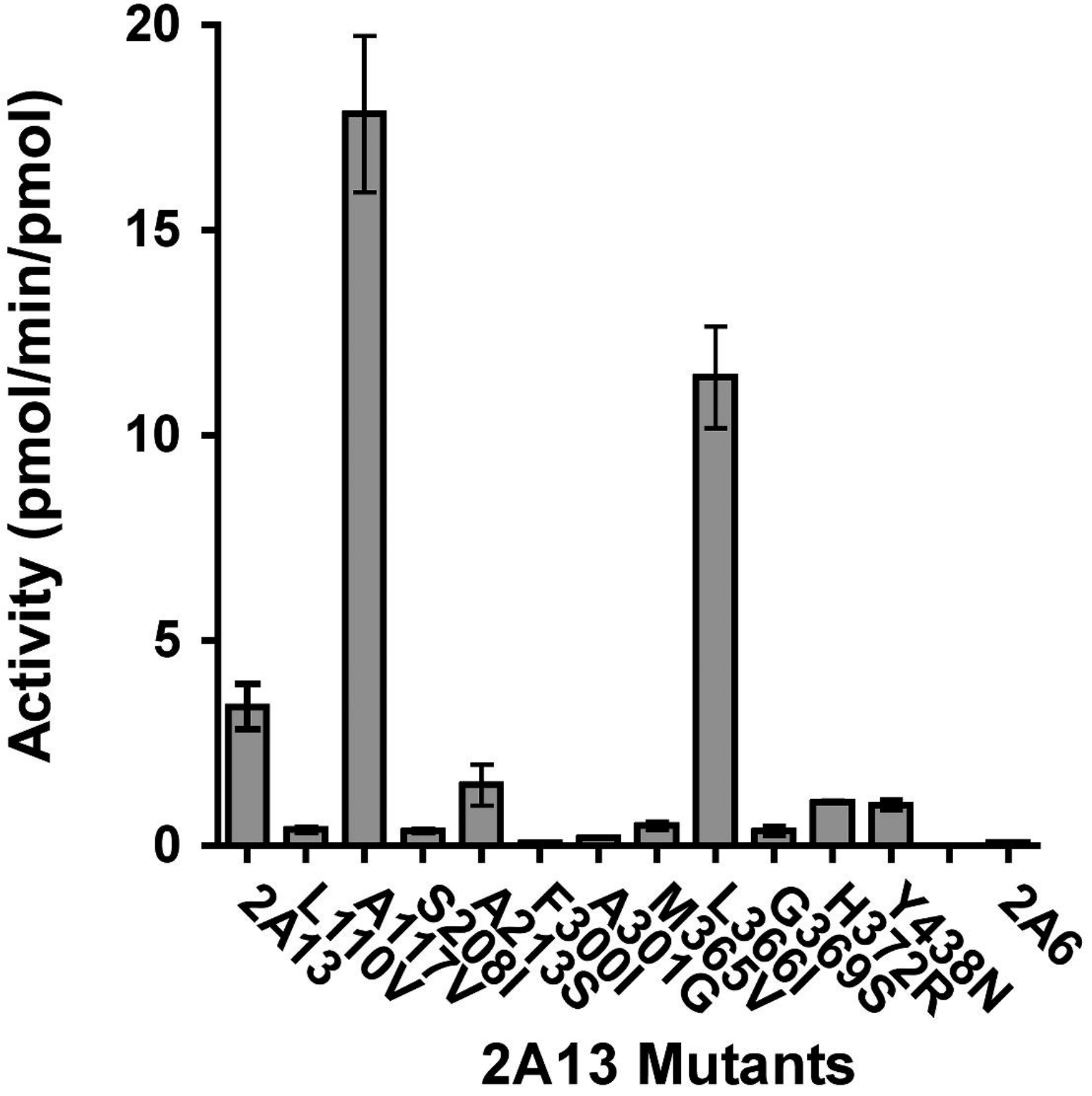
20
15
10
5
0
Activity (pmol/min/pmol)
2A13
L110V
A117V
S208I
A213S
F300I
A301G
M365V
L366I
G369S
H372R
Y438N
2A6
2A13 Mutants

Figure 3

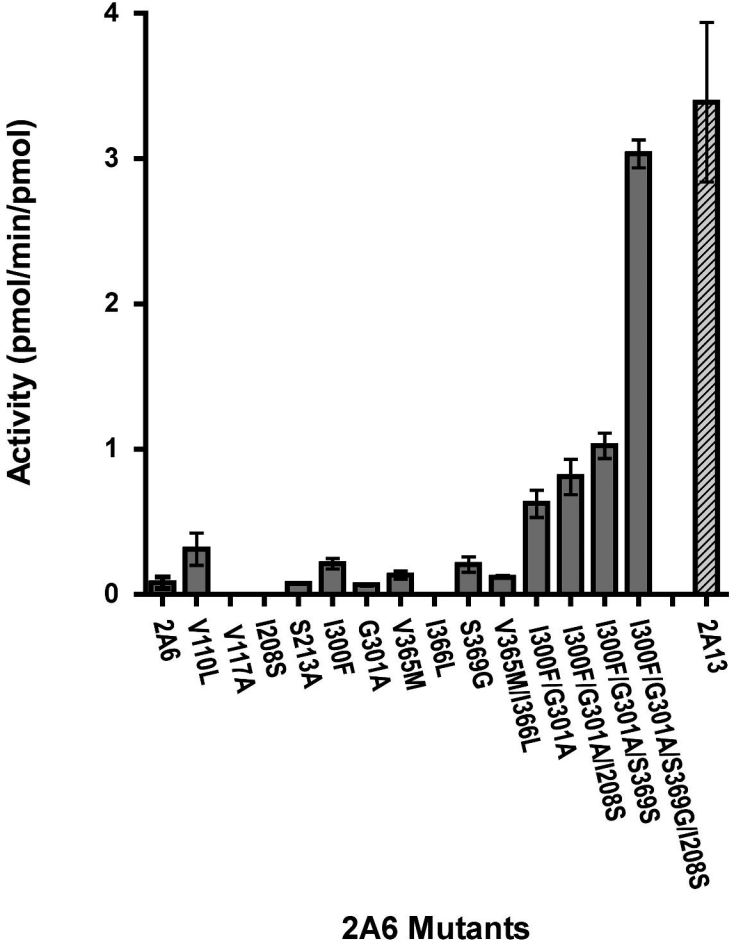
Activity (pmol/min/pmol)
0
1
2
3
4
2A6
V110L
V117A
I208S
S213A
I300F
G301A
V365M
I366L
S369G
V365M/I366L
I300F/G301A
I300F/G301A/I208S
I300F/G301A/S369S
I300F/G301A/S369G/I208S
2A13
2A6 Mutants

Figure 4

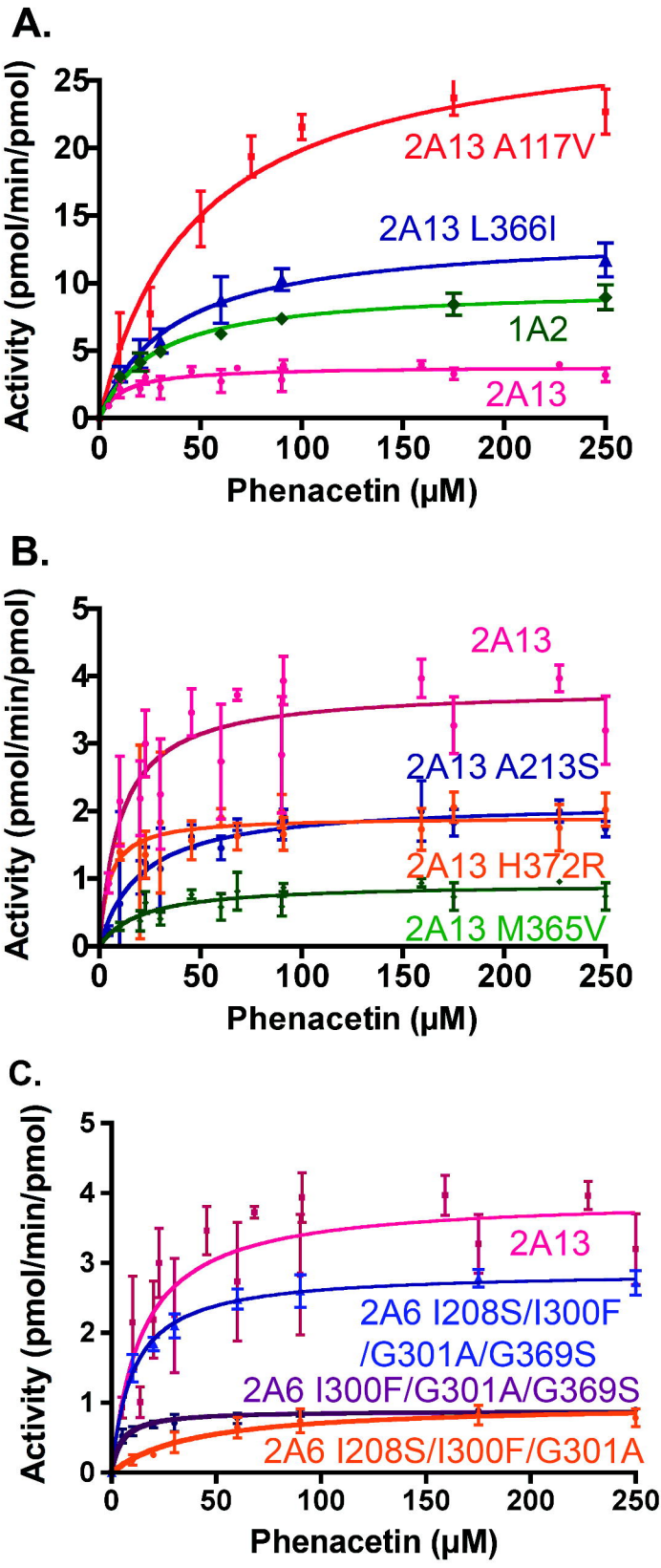
A.
Activity (pmol/min/pmol)
25
20
15
10
5
0
0
50
100
150
200
250
Phenacetin (μM)
2A13 A117V
2A13 L366I
1A2
2A13
B.
Activity (pmol/min/pmol)
5
4
3
2
1
0
0
50
100
150
200
250
Phenacetin (μM)
2A13
2A13 A213S
2A13 H372R
2A13 M365V
C.
Activity (pmol/min/pmol)
5
4
3
2
1
0
0
50
100
150
200
250
Phenacetin (μM)
2A13
2A6 I208S/I300F
/G301A/G369S
2A6 I300F/G301A/G369S
2A6 I208S/I300F/G301A

Figure 5

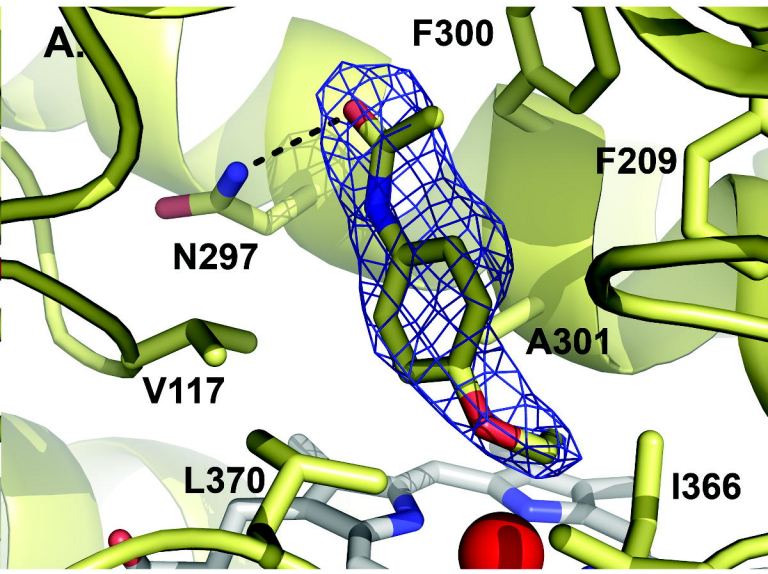
A.
F300
F209
N297
A301
V117
L370
I366

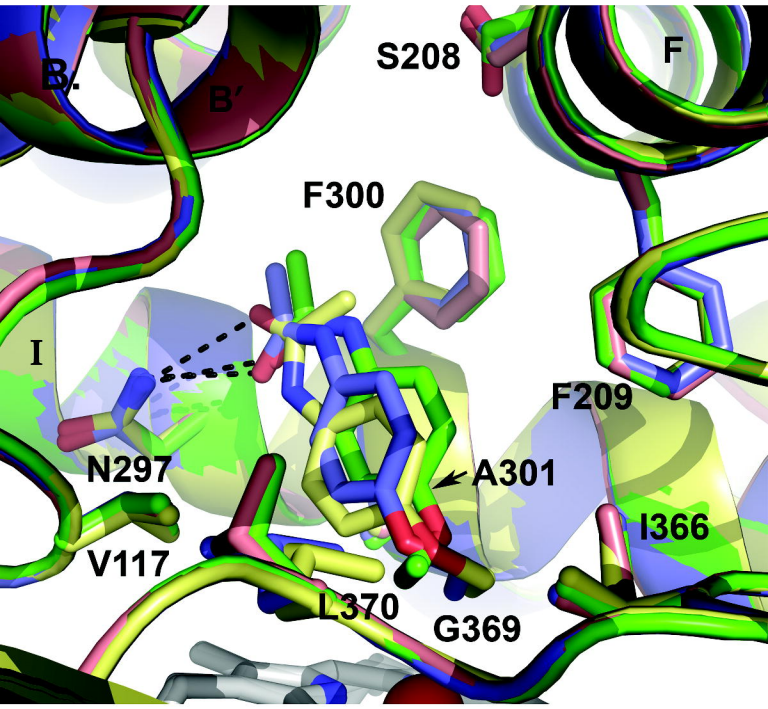
B.
B′
S208
F
F300
I
F209
N297
A301
I366
V117
L370
G369

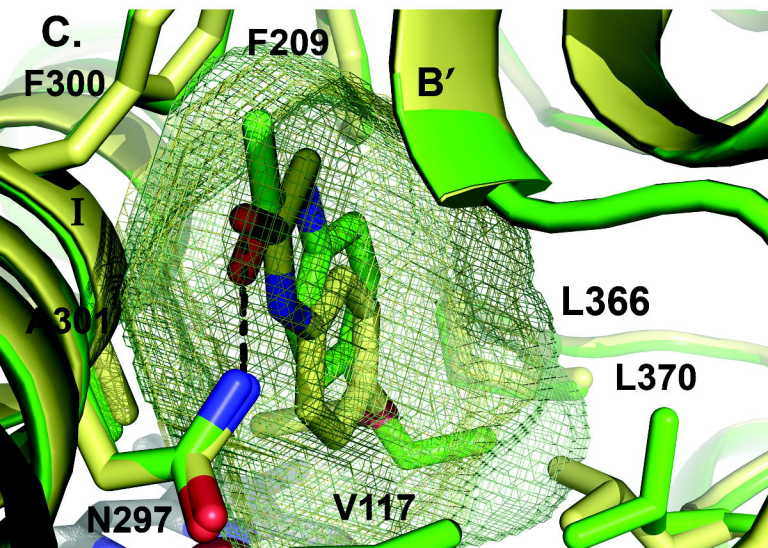
C.
F209
F300
B′
I
L366
A301
L370
N297
V117

Figure 6

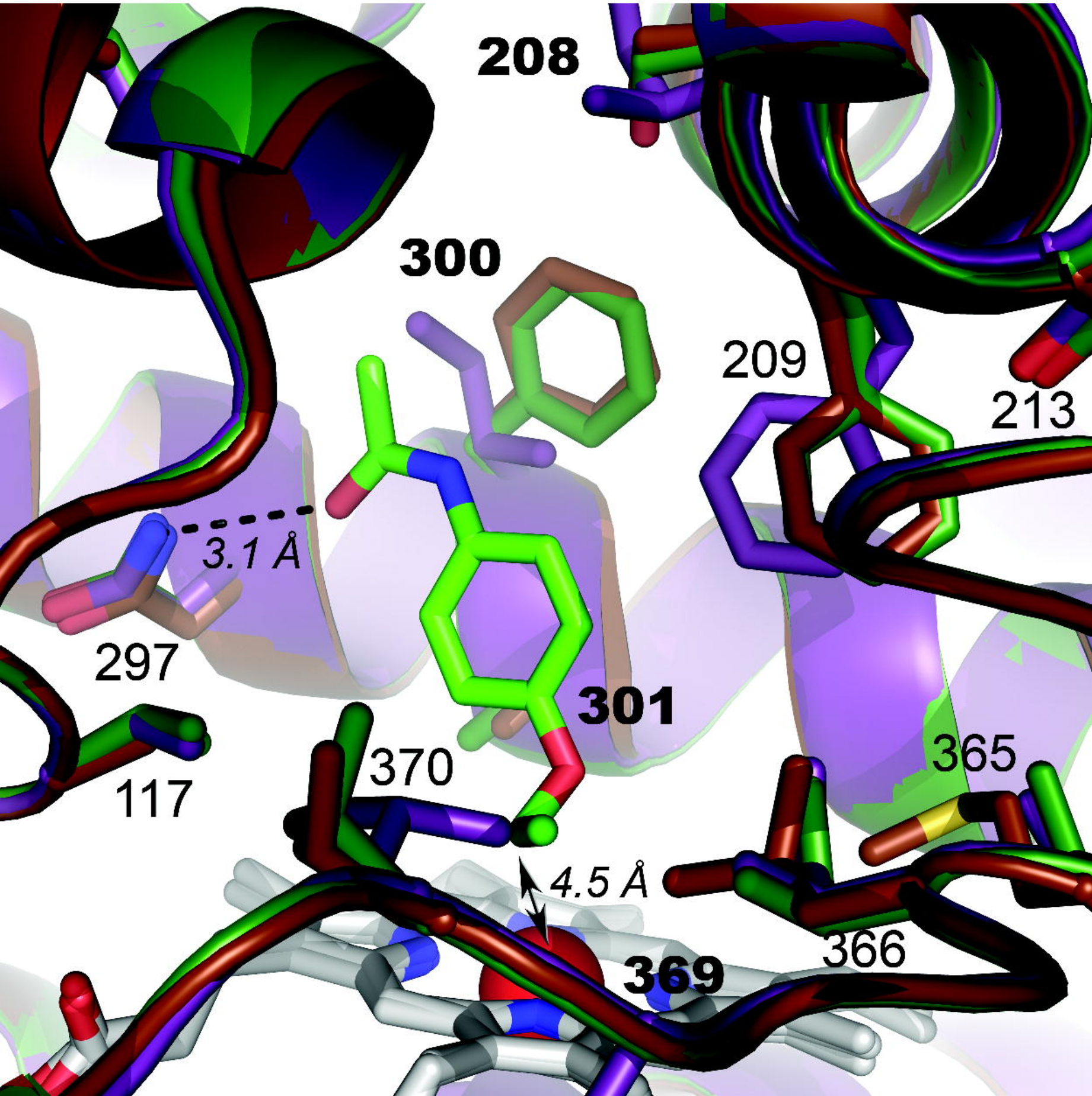

Figure 7